International Journal of Precision Engineering and Manufacturing (2019) 20:619–630
https://doi.org/10.1007/s12541-019-00030-2

Online ISSN 2005-4602
Print ISSN 2234-7593

REGULAR PAPER

Design for Powder Metallurgy: Predicting Anisotropic Dimensional Change on Sintering of Real Parts

I. Cristofolini[1] · A. Molinari[1] · M. Zago[1] · S. Amirabdollahian[1] · O. Coube[2] · M. J. Dougan[3] · M. Larsson[4] · M. Schneider[5] · P. Valler[6] · J. Voglhuber[7] · L. Wimbert[5]

Received: 31 May 2018 / Revised: 9 January 2019 / Accepted: 23 January 2019 / Published online: 4 March 2019

Abstract

Anisotropic dimensional change on sintering may strongly affect the precision of parts produced by press and sinter. In previous work a design procedure accounting for anisotropic dimensional change of axi-symmetric parts (disks and rings) has been developed on the basis of experimental data. In this work the procedure has been applied to predict the anisotropic dimensional change of real parts produced in industrial conditions, providing that coaxial rings were identified in the geometry of the actual parts. Parts were highly different for material, complexity of geometry, green density and process conditions. Parts were measured in the green and sintered state and the measured dimensional changes were compared to the predicted ones, finding a good agreement. The procedure was also adapted to predict dimensional change of an oval feature, and highly satisfactory results were obtained.

Keywords Anisotropy · Dimensional change · Powder metallurgy · Precision of PM parts

List of symbols

h	Height of the part (mm)
h_g	Height of the green part (mm)
h_s	Height of the sintered part (mm)
ε_h	Dimensional change in height
ϕ_{ext}	External diameter (mm)
$\phi_{ext\ g}$	External diameter of the green part (mm)
$\phi_{ext\ s}$	External diameter of the sintered part (mm)
$\varepsilon_{\phi\ ext}$	Dimensional change in the external diameter
ϕ_{int}	Internal diameter of the part (mm)
$\phi_{int\ g}$	Internal diameter of the green part (mm)
$\phi_{int\ s}$	Internal diameter of the sintered part (mm)
$\varepsilon_{\phi\ int}$	Dimensional change in the internal diameter
ε_{iso}	Isotropic dimensional change
V_g	Volume of the green part (mm^3)
V_s	Volume of the sintered part (mm^3)
R	Ratio between the internal and the external diameter in the green parts
α	Geometrical parameter relating the dimensional changes
γ	Geometrical parameter relating R and α
K	Anisotropy parameter

✉ I. Cristofolini
ilaria.cristofolini@unitn.it

[1] Department of Industrial Engineering, University of Trento, Via Sommarive, 9, 38123 Trento, Italy

[2] European Powder Metallurgy Association, 2nd Floor, Talbot House, Market Street, Shrewsbury SY1 1LG, UK

[3] AMES Barcelona Sintering S.A., Camí de Can Ubach, 8, Pol. Ind. "Les Fallulles", 08620 Sant Vicenç dels Horts, Barcelona, Spain

[4] Höganäs AB, Bruksgatan 35, 263 83 Höganäs, Sweden

[5] GKN Sinter Metals Engineering GmbH, Krebsöge 10, 42477 Radevormwald, Germany

[6] Sintex a/s, Jyllandsvej 14, 9500 Hobro, Denmark

[7] MIBA Sinter Austria GmbH, Dr.-Mitterbauer-Str. 1, 4655 Vorchdorf, Austria

1 Introduction

Anisotropic dimensional change on sintering is a critical aspect to be considered designing parts produced by press and sinter. Considering axi-symmetric ring shaped parts, not only dimensional change in the compaction plane may significantly differ from that along the axial direction, but even dimensional change of the internal diameter may be different from dimensional change of the external diameter, as by previous investigation [1]. The phenomenon has been extensively studied by the authors at the University

of Trento, dealing with the many different variables, which determine it.

The influence of material is critical on change in volume: shrinking or swelling, and their amount, mainly derive from chemical composition, and anisotropy of dimensional changes is highly affected too. The behaviour of parts made up of Fe–Cu–P [2], Fe–Cu–C [3, 4], Fe–Cr–Mo–C [5] was investigated in previous work, and the influence of copper and phosphorus on pure iron was highlighted and compared in [6, 7]. Process parameters also strongly affect anisotropic dimensional change on sintering, as highlighted by the studies comparing parts sintered at standard sintering temperature and parts high-temperature sintered [8–11]. As by several authors [12–17], material and process parameters determine the different mechanisms occurring during sintering, among them the occurrence of solid state sintering or liquid phase sintering, which also strongly affect anisotropy of dimensional changes and were investigated in depth [18–23]. According to Zavaliangos and Bouvard [24, 25], deformation of particles by prior cold compaction has been observed as one of the main causes of anisotropy [26–30]. Olewsky [31] and Bordia et al. [32] proposed a theory for anisotropic shrinkage based on deformation of powder particles, which determines anisotropic orientation of pores. Wakai et al. [33, 34], according to the continuum solid mechanics approach, described anisotropic sintering shrinkage on the basis of the relationships between sintering stress and strain rate, as by the anisotropic particle packing and their rearrangement during sintering.

Aiming at applying the knowledge gained on anisotropy of dimensional changes to real parts, the influence of geometry was investigated, focusing the attention on axi-symmetric parts (disks and rings characterised by different H/D and H/($D_{ext} - D_{int}$), respectively) [6, 32]. On the basis of the experimental results, aiming at predicting dimensional changes, as in Raman et al. [36], an analytical model for the anisotropic dimensional change on sintering of ferrous axi-symmetric parts was developed [1, 37], from which the design procedure [38] used in the present work.

This work applies the design procedure to predict the anisotropic dimensional change of real parts produced in industrial conditions. The parts differ for material, complexity of geometry, green density, and process conditions, thus representing a demanding test-bed for the design procedure and a good opportunity to identify guidelines for future work.

2 Experimental Procedure

Aiming at broadly investigating dimensional change on sintering, the five industrial parts shown in Fig. 1 have been considered in this work, differing for material, geometry, size, and production process. All of them were produced in standard industrial conditions.

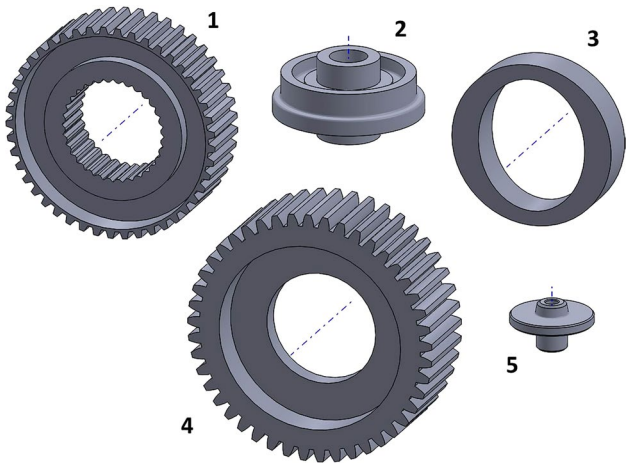

Fig. 1 The parts studied

Table 1 Main dimensions of the different parts

Part	D_{min} (mm)	D_{max} (mm)	H_{min} (mm)	H_{max} (mm)
1	37	81	7	23
2	10	55	5	30
3	40	60	–	18
4	42	94	6	30
5	5	30	4	18

Table 1 reports the approximate smallest (D_{min}, H_{min}) and largest dimensions (D_{max}, H_{max}) recognizable in the different parts, referring to Fig. 2.

Seven to ten parts for each material/geometry have been measured by a CMM, according to the measurement procedure following described. The same part has been measured in the green and sintered state, aiming at minimizing the influence of noise factors on the evaluation of dimensional changes. Dimensions have been derived from geometrical features, namely: heights from the distance of two parallel planes (the planes were obtained by minimum least square method applied to the points measured by continuous scan [39] on the related flat surfaces), diameters from cylindrical surfaces (the cylinders were obtained by minimum least square method applied to the circles measured by continuous scan at different levels). In some cases the diameters measured at different levels showed a trend, which was related to the influence of the compaction step, as explained in the following. Gear teeth were considered as defined by two cylindrical features, obtained from the points measured at the base and at the top of the teeth at different levels.

The chemical composition and the green density are summarized in Table 2.

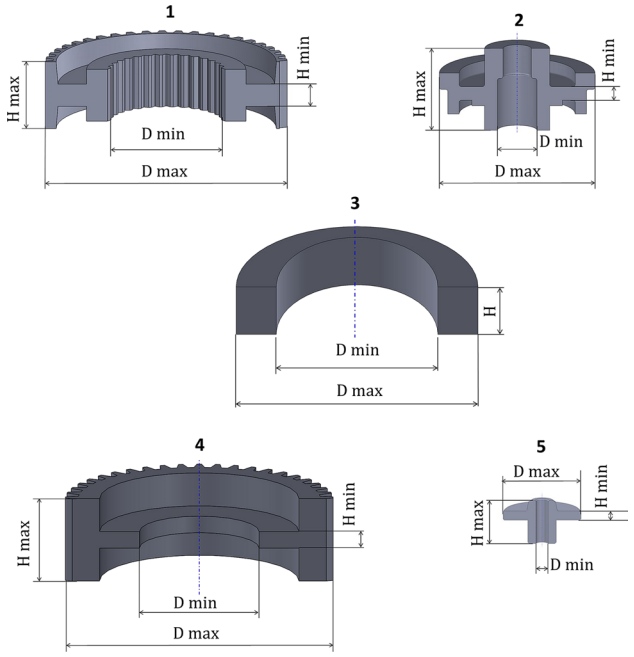

Fig. 2 Minimum and maximum dimensions of the parts studied

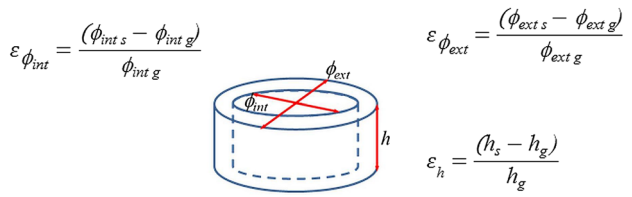

Fig. 3 Dimensional changes for a ring

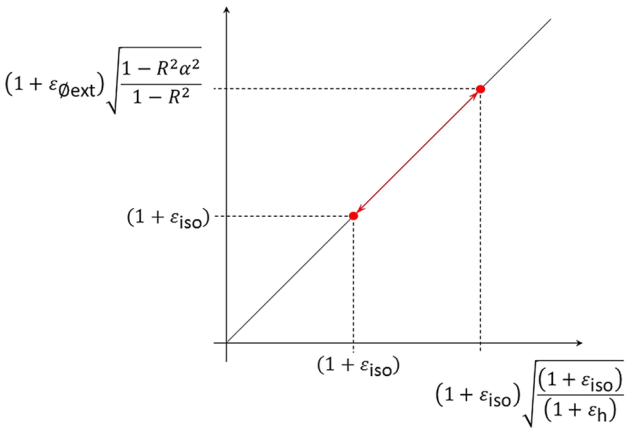

Fig. 4 Anisotropic versus isotropic dimensional change

3 Anisotropy Parameter *K*

In previous work [6] the anisotropy parameter K has been defined, aiming at quantitatively describing the anisotropy of dimensional changes, main steps are here shortly resumed. Dimensional change on sintering is due to change in volume, as by the relationship in Eq. (1), referring to a ring (see Fig. 3)

$$1+\frac{V_s-V_g}{V_g}=\left(1+\varepsilon_h\right)\frac{(1+\varepsilon_{\phi\,ext})^2-R^2(1+\varepsilon_{\phi\,int})^2}{1-R^2}$$
$$R=\frac{\phi_{\text{int}\,g}}{\phi_{ext\,g}} \tag{1}$$

Aiming at identifying a reference parameter to quantify anisotropy, the isotropic dimensional change has been considered, which is related to the change in volume by Eq. (2)

$$1+\frac{V_s-V_g}{V_g}=(1+\varepsilon_{iso})^3 \tag{2}$$

The anisotropy parameter K comes from the relationships above, relating the actual anisotropic dimensional changes to the reference isotropic dimensional change, through the change in volume, as by Eq. (3), where the dimensional change in the compaction plane lies on the right and the dimensional change in the axial direction on the left

$$\frac{\left(1+\varepsilon_{iso}\right)^3}{(1+\varepsilon_h)}=\frac{(1+\varepsilon_{\phi ext})^2-R^2\alpha^2(1+\varepsilon_{\phi ext})^2}{1-R^2}=(1+\varepsilon_{\phi ext})^2\frac{1-R^2\alpha^2}{1-R^2} \tag{3}$$

where $\alpha=\frac{1+\varepsilon_{\phi\text{int}}}{1+\varepsilon_{\phi ext}}$.

Plotting the entities in Eq. (3) on the graph shown in Fig. 4, the points relevant the different dimensional changes will lie on the bisector line, and the far they will be from

Table 2 Chemical composition and green density

Part	Material	Green density (g/cm^3)
1	2% Cu, 1.5% Mo, Fe balance + 0.6% C	6.93–7.03
2	Ancorsteel DWP200—12%FD10Cu + 0.65%C	7.0
3	AISI 430L	6.30–6.45
4	1.8%Cr, 1% Cu, Fe balance + 0.6% C	7.15
5	AISI 316L	6.25–6.45

the point relevant to the isotropic dimensional changes, the larger the anisotropy of dimensional changes.

Through the distance highlighted in Fig. 4, related to the isotropic dimensional change, the anisotropy parameter K is defined by Eq. (4), where $\gamma = \sqrt{\frac{1-R^2\alpha^2}{1-R^2}}$

$$K = \frac{(1+\varepsilon_{\phi ext})\gamma - (1+\varepsilon_{iso})}{\varepsilon_{iso}} \tag{4}$$

K has been experimentally derived as a function of the isotropic dimensional change measuring, in the green and sintered state, the dimensions of disks and rings showing different diameters and heights, obtained by different materials in different process conditions. The study has been carried out step by step, so that the functions best fitting the data related to small and large change in volume have been found to be different, as shown in Fig. 5 (see references [1] and [6] for explanation in depth).

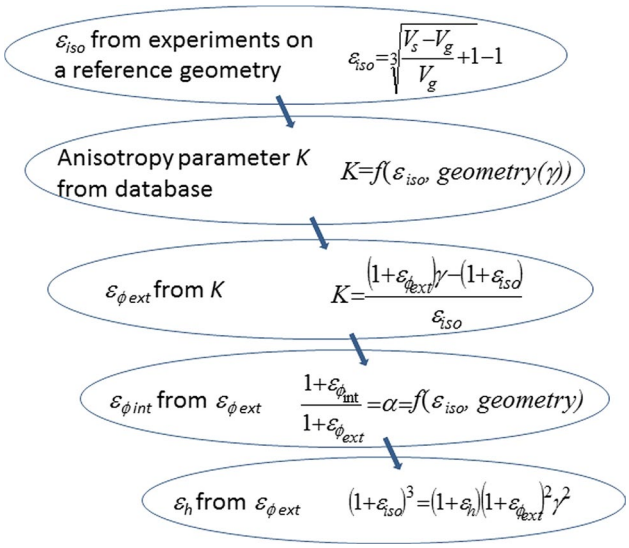

Fig. 6 The design procedure aimed at predicting anisotropic dimensional changes

4 The Design Procedure

A design procedure aimed at predicting the anisotropic dimensional changes on sintering of ring shaped parts has been proposed, on the basis of the anisotropy parameter K. Main steps are summarized in Fig. 6.

The isotropic dimensional change, which is directly related to the change in volume, is the starting point of the design procedure. In this project very different materials and geometries were considered, so that the isotropic dimensional change has been derived from measurement of the green and sintered parts. However, future development aims at identifying classes of materials/reference geometries/production processes to establish a database of isotropic dimensional changes to be directly used in the design procedure. The procedure allows predicting the dimensional changes of a ring providing that K and α parameters are known (see references [1] and [6] for explanation in depth).

The procedure above is related to a single ring, the application on real parts implies the identification of coaxial rings in the real axi-symmetric parts. As shown in Fig. 7, coaxial rings can be identified by a "column based approach" (referring to the powder columns, which can be identified during

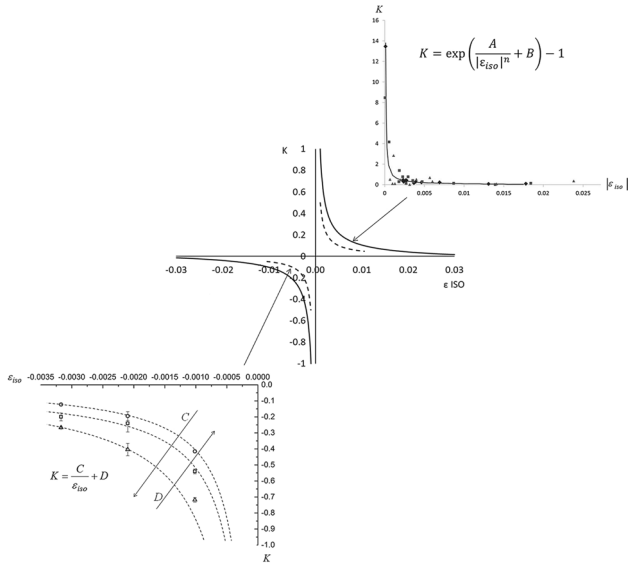

Fig. 5 Anisotropy parameter K as a function of the isotropic dimensional change

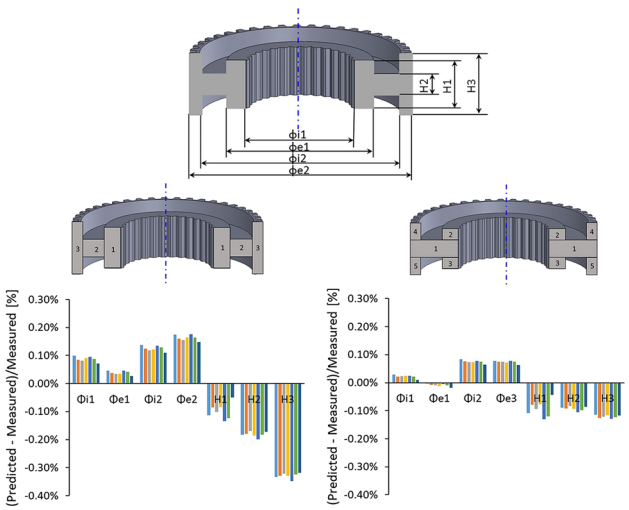

Fig. 7 Comparison between "column based approach" and "maximum section based approach"

uniaxial compaction) or by a "maximum section based approach" (referring to the maximum amount of shrinking/swelling material, which drags after the other rings). Congruency among the dimensional changes of diameters common to the different rings is ensured. See Ref. [35] for explanation in depth.

Figure 7 also shows the difference between the dimensional change predicted by the procedure above (as calculated by the two different approaches) and the dimensional change measured on the real parts; each bar corresponds to one of the measured parts. The better effectiveness of "maximum section based approach" is confirmed, so that it will be used to predict the dimensional changes from here on.

5 Results and Discussion

For each part, coaxial rings determining the whole geometry have been distinguished, according to the maximum section based approach, as shown in Fig. 8.

Slightly conical surfaces have been represented by two slightly different coaxial cylindrical surfaces, as shown by parts 1 and 5. Part 3 represents a particular case, being the hole oval, and will be presented singularly, as the peculiar case of application of the design procedure to non-cylindrical surfaces. In the case of gears, the external ring has been considered both by the enveloping cylinder (top of the teeth) and by the cylinder at the base of the teeth, obtaining similar results.

The application of the design procedure allowed determining the predicted dimensional change for all the dimensions defining the coaxial rings in Fig. 8, providing the necessary congruencies among dimensions common to different entities (for example, the dimensional change of the internal diameter is supposed to be equal in all the rings with the same hole). Predicted dimensional changes were then compared with measured dimensional changes.

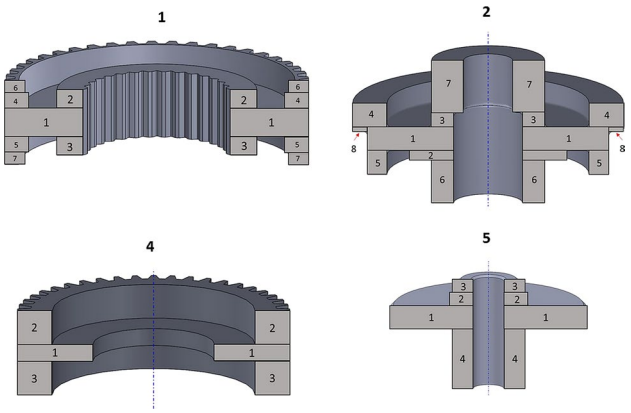

Fig. 8 Parts splitting as by maximum section based approach

Results are presented grouping parts showing small change in volume, namely parts 1, 2, and 4 (and consequently small isotropic dimensional change, that is −0.0018, 0.0005, and 0.0012) and parts showing large change in volume, namely parts 3 and 5 (and consequently large isotropic dimensional change, −0.024 and −0.025).

The results will be presented grouping dimensions by size, showing both the difference between the predicted and measured dimensional change, and the same difference referred to the measured dimensional change, to obtain a value in percentage terms.

5.1 Parts Showing Small Change in Volume

The difference between predicted and measured dimensional change of internal diameters, both in absolute values (upper side) and in percentage terms (lower side) is shown in Fig. 9.

The difference increases on increasing the nominal dimension, but in percentage terms it is always lower than 0.15%, thus meaning a generally good precision in predicting dimensional changes.

In some cases a different behaviour is observed when considering dimensions, which are nominally the same, but are related to features closer to the bottom or the upper punch in compaction, features B and T in Fig. 9, respectively. The trend, however, is not necessarily verified, as by Fig. 6, and might be attributed to the compaction strategy and/or to the orientation of parts in the sintering furnace.

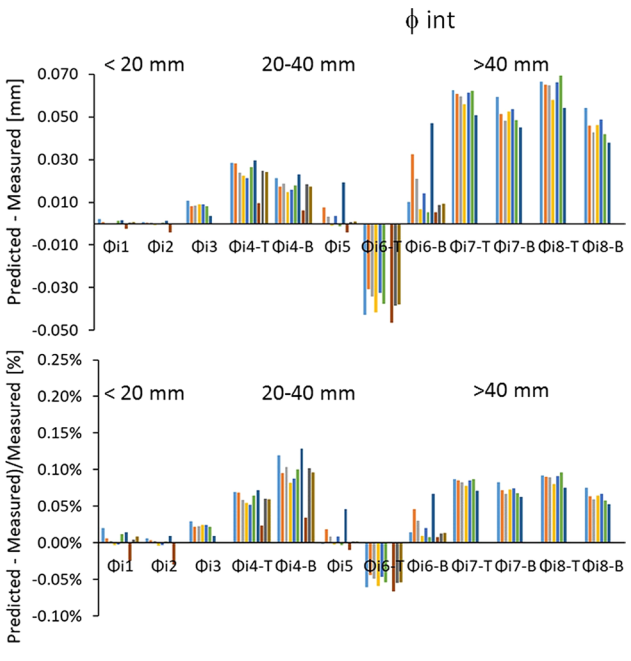

Fig. 9 Difference between predicted and measured dimensional change of internal diameters, both in absolute values (upper side) and in percentage terms (lower side)

Figures 10 and 11 show the difference between predicted and measured dimensional change of external diameters and heights, respectively, both in absolute values (upper side) and in percentage terms (lower side).

As shown in Fig. 10, dimensional change of external diameters is predicted even more precisely than that of internal ones, while a slightly lower precision is observed in prediction of dimensional change of heights. However, it must be observed that the largest differences between predicted and measured dimensional changes are related to the dimensions of the part with the lowest isotropic dimensional change (0.0005, practically negligible).

The anisotropy parameter K used in the design procedure is defined by a ratio with the isotropic dimensional change at denominator (Eq. 4), what may imply a strong effect when the isotropic dimensional change is close to zero. As a general remark, the precision of dimensional change prediction of parts with small change in volume is good, apart from two single heights the difference between predicted and measured dimensional change is lower than 0.15%.

5.2 Parts Showing Large Change in Volume

The difference between predicted and measured dimensional change of internal and external diameters, both in absolute values (upper side) and in percentage terms (lower side) is shown in Fig. 12.

The difference generally increases on increasing the nominal dimension, but not necessarily. In percentage terms it is always larger than in parts showing small change in volume, around 0.25% rather than 0.15%, thus meaning a decrease of precision in predicting dimensional changes.

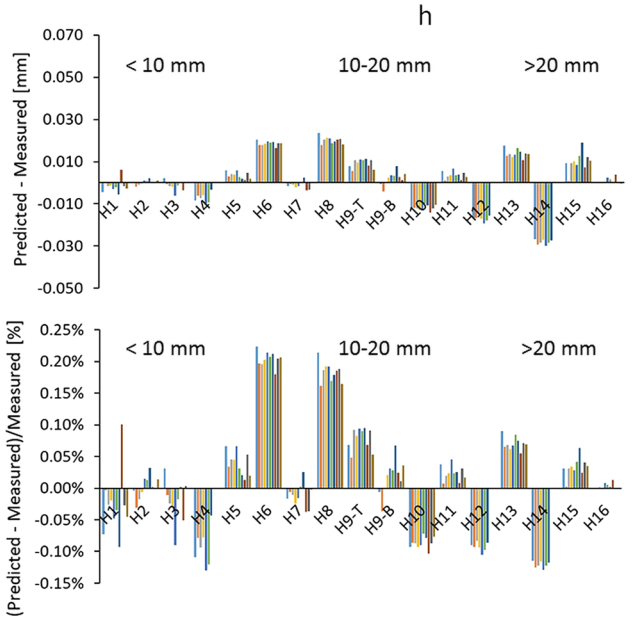

Fig. 11 Difference between predicted and measured dimensional change of heights, both in absolute values (upper side) and in percentage terms (lower side)

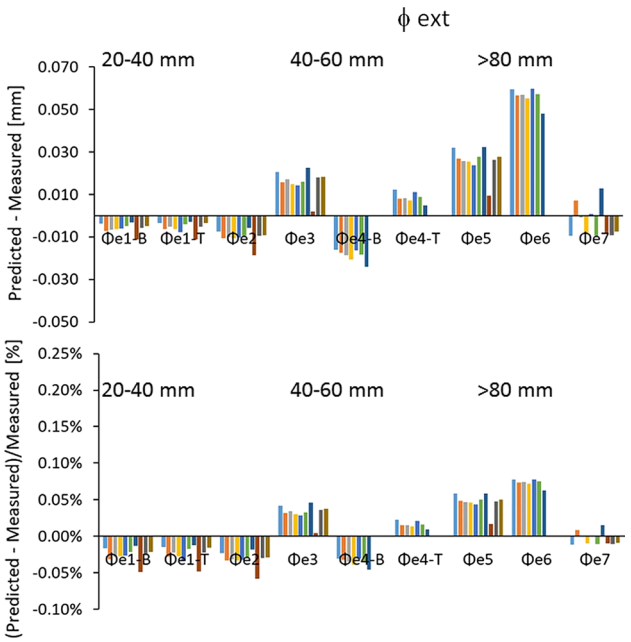

Fig. 10 Difference between predicted and measured dimensional change of external diameters, both in absolute values (upper side) and in percentage terms (lower side)

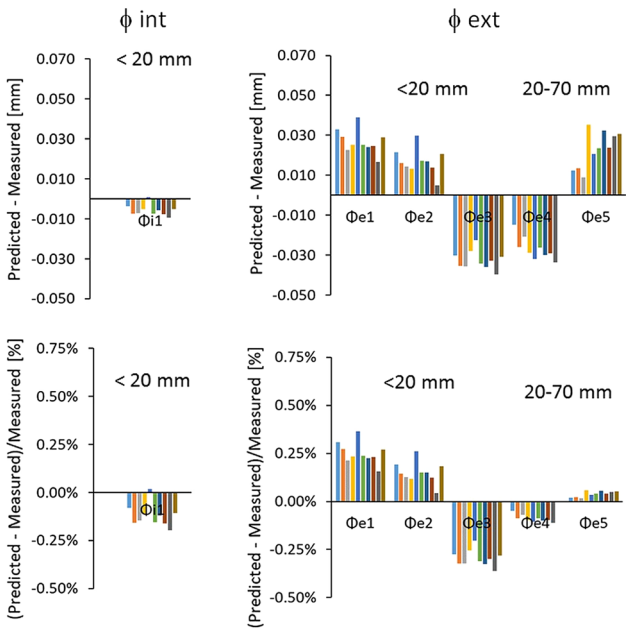

Fig. 12 Difference between predicted and measured dimensional change of internal and external diameters, both in absolute values (upper side) and in percentage terms (lower side)

Concerning heights, the difference between predicted and measured dimensional change, both in absolute values (upper side) and in percentage terms (lower side), is shown in Fig. 13.

The worsening in predicting dimensional change observed for diameters is even larger for heights, where the difference between predicted and measured dimensional change is up to 0.75%. The design procedure is less reliable in predicting dimensional change of parts with large change in volume. The reason for this worsening has to be ascribed to parameters (both geometrical and process related) determining the anisotropy parameter *K*, which are experimentally derived. In previous experiments, in fact, the sampling showing large change in volume encountered liquid phase sintering, while in the present work, as well as in previous experiments determining small change in volume, always solid phase sintering occurs. Consequently, the mechanisms occurring during sintering are completely different, and they likely affect the anisotropic dimensional change. Further work will imply a wider sampling, to enlarge and strengthen the reference database.

5.3 Dimensional Change of Non-cylindrical Features

Part shown in Fig. 14 has an oval hole defined by two axes, namely $\phi_{i\,min}$ and $\phi_{i\,max}$.

The design procedure has been developed referring to cylindrical features, so that the part above has been firstly approached as it was a cylinder with a cylindrical hole, under the hypothesis of three different diameters, $\phi_{i\,min}$, $\phi_{i\,max}$, and an average diameter given by $(\phi_{i\,min}+\phi_{i\,max})/2$, respectively. In all the cases results were disappointing, leading to a strong underestimation of the minimum axis and a strong overestimation of the maximum axis, as shown in Fig. 15.

A function representing the whole profile has thus been considered, derived from the points measured by continuous scan on the green and sintered surfaces of the hole. However, it is not possible to compare the data points by points, since the angular position of the data acquired are not perfectly coincident. This means that the data of the inner scan of the green part cannot be used directly in the model, so that an analytical curve, fitting the points of green and sintered

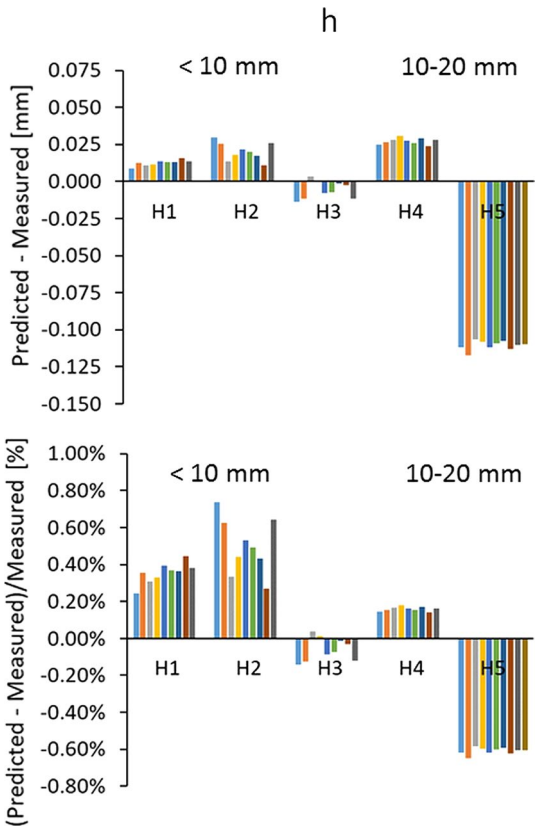

Fig. 13 Difference between predicted and measured dimensional change of heights, both in absolute values (upper side) and in percentage terms (lower side)

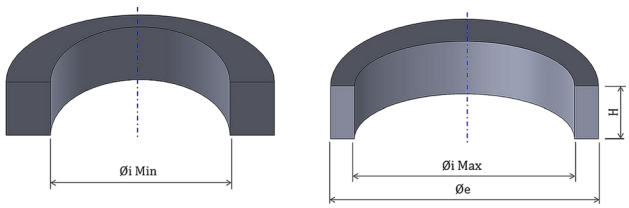

Fig. 14 Dimensions of features in part 3

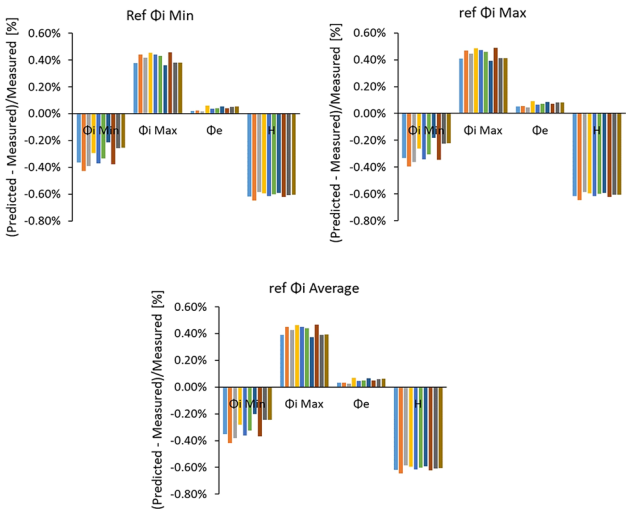

Fig. 15 Difference between predicted and measured dimensional changes as obtained considering part 3 as a ring with a cylindrical hole (different diameters)

scans was used to compare the values at the same position, as shown in Fig. 16.

The fitting function used is Eq. (5)

$$\left(\frac{X}{a}\right)^n + \left(\frac{Y}{b}\right)^n = 1 \tag{5}$$

Same as Eq. (6) in polar coordinates

$$\left(\frac{\rho * \cos\theta}{a}\right) + \left(\frac{\rho * \sin\theta}{b}\right) = 1 \tag{6}$$

where a and b are the semi axes of the curve previously measured. The parameter determined by the fitting equation is the exponential n, which is very close to 2, so that the oval might be reasonably approximated by an ellipse.

Nevertheless, even using the function representing the profile, instead of the single values of the axes, a nearly negligible improvement was obtained, as by Fig. 17. Again, the minimum axis was strongly underestimated and the maximum axis strongly overestimated.

However, the dimension and its angular position corresponding to the minimum difference between the predicted and measured dimensions was identified, which corresponds to the equivalent radius R_{eq} of the circular hole of the ring having the same volume of the part, as it was verified. Referring to the difference between the inner radius and the equivalent radius, as in the abscissa axis of the graph plotted in Fig. 18, a corrective function well fitting the difference

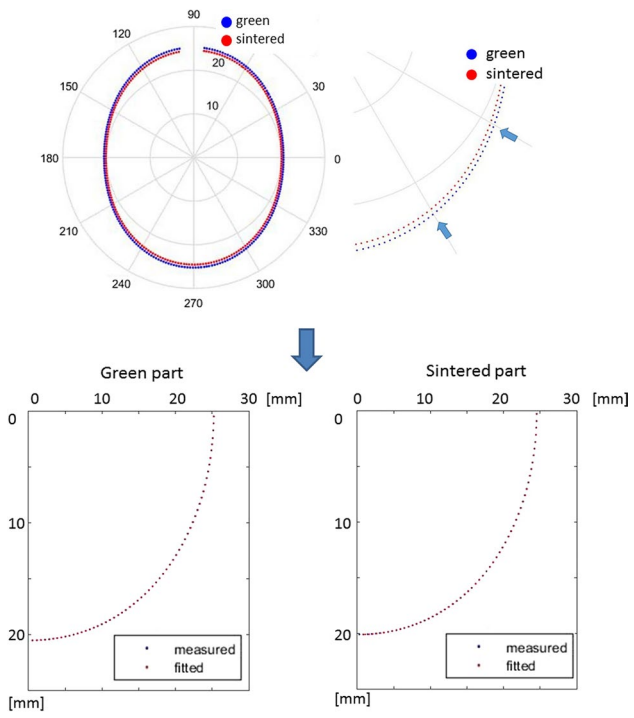

Fig. 16 Scan points of green and sintered parts and fitting functions

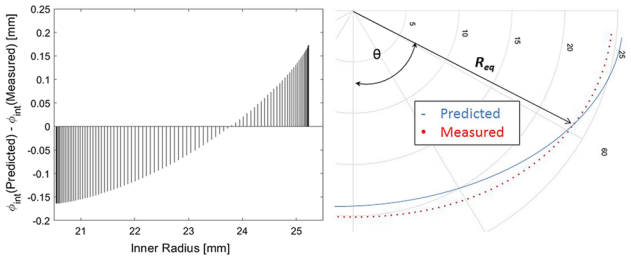

Fig. 17 Difference between predicted and measured internal "diameter" in the different positions

between predicted and measured internal dimension has been identified.

The corrective function (Eq. 7) was used to determine a new predicted dimension (as by Eq. 8), and consequently a new difference between the predicted and measured dimension

$$\phi_{int}(Predicted) - \phi_{int}(Measured) = 0.015 \cdot (R - R_{eq})^2 + 0.094(R - R_{eq}) \tag{7}$$

$$\phi_{int}(Pred\_corr) = \phi_{int}(Predicted) - \left[0.015 \cdot (R - R_{eq})^2 + 0.094 \cdot (R - R_{eq})\right] \tag{8}$$

The corrective function was applied to the whole data, and it allowed to strongly cut the difference between the predicted and the actual dimensions. Examples are shown in Fig. 19.

This difference is always included in the interval (−0.05/+0.05), representing the required dimensional tolerance for the minimum and maximum «diameters» of the oval hole, as summarized in Fig. 20.

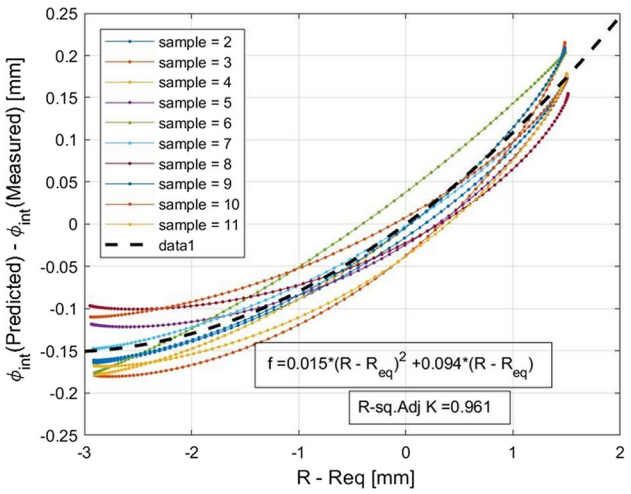

Fig. 18 Difference between predicted and measured internal "diameter" as a function of the difference between the "radius" and the equivalent radius—measured data and fitting function

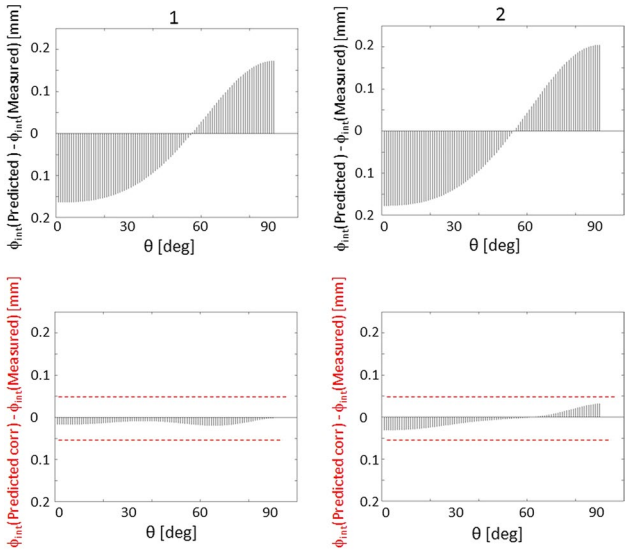

Fig. 19 Examples of the difference between predicted and measured internal "diameter" in the different positions without corrective function (upper) and with corrective function (lower)

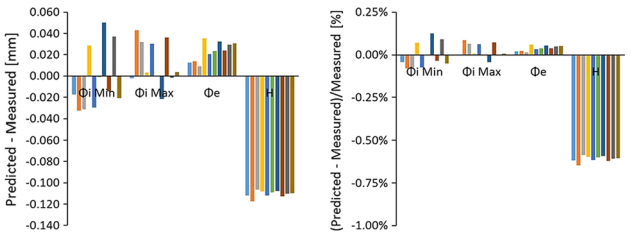

Fig. 20 Difference between predicted and measured dimensional changes—effect of corrective function

5.4 Predicted Dimensional Changes and Tolerance Classes

From the designer point of view, the effectiveness of the procedure can be evaluated from the ISO tolerance class related to the difference between predicted and measured dimension. Figure 21 summarizes the mean values for ISO IT classes derived from the difference between predicted and measured dimensions for all the parts studied, showing both small and large change in volume. The ISO IT classes have been grouped by internal diameter, external diameter, and height, distinguishing the different size intervals.

It may be observed that there is no direct correlation between the size of the dimension and the allowable dimensional tolerance, neither an influence of the compaction direction can be highlighted.

The ISO IT class related to the difference between predicted and measured dimensions never exceeds ISO IT 9, and in most of the cases it is very low, belonging to the

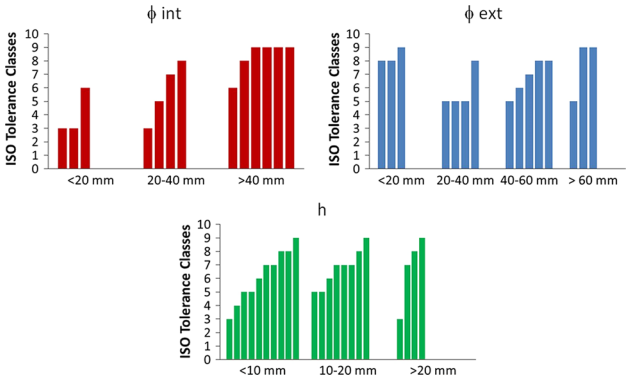

Fig. 21 ISO IT classes derived from the difference between predicted and measured dimensions for the different features

interval IT3/IT7. These results are reasonably good from the designer point of view, considering the tolerance classes generally related to press and sinter (IT10–IT12).

Nevertheless, it must be honestly admitted that in this way part of the allowed tolerance is consumed by the uncertainty in prediction. Work is in progress aiming at furtherly lowering the tolerance classes, so that the procedure actually becomes a design tool ensuring high precision of industrial parts.

6 Conclusions

This work investigated the effectiveness of the design procedure accounting for anisotropic dimensional changes developed in previous work. Five axi-symmetric industrial parts were considered, differing for material, geometry, and production process. Main results are here summarised.

- The dimensional changes of parts showing small change in volume were predicted with good accuracy, the difference between predicted and measured dimensional change never exceeded 0.15%, being lower in most of the cases. The dimensional changes of parts showing large change in volume were less precisely predicted, particularly concerning dimensions in the axial direction. The difference between predicted and measured dimensional change of diameters did not exceed 0.25%, while it was up to 0.75% for what concerns heights. The reason for this worsening was ascribed to parameters (both geometrical and process related) determining the anisotropy parameter K, which are experimentally derived from sampling encountering liquid phase sintering, while in the present work always solid phase sintering occurs. Consequently, the mechanisms occurring during sintering are completely different, and they likely affect the anisotropic dimensional change.

- Nevertheless, results are reasonably good from the designer point of view. In terms of tolerances, the difference between predicted and measured dimension never exceeded IT 9, corresponding to the worst cases, while in most of the cases it belonged to the interval IT3–IT6.
- Influence of compaction on anisotropic dimensional changes has been highlighted, likely due to compaction/ejection strategy and to the consequent density gradient.
- Concerning non-cylindrical features (oval hole), a corrective function has been identified allowing a very accurate and precise prediction of dimensional change.

This work also highlighted directions for improvement, mainly aimed at enlarging and strengthening the reference database, for example with relationship to large isotropic dimensional change obtained by solid state sintering, and to different geometries, thus improving the effectiveness of the design procedure.

References

1. Cristofolini, I., Corsentino, N., Larsson, M., & Molinari, A. (2016). Analytical model of the anisotropic dimensional change on sintering of ferrous pm parts. *Powder Metallurgy Progress, 16*(1), 27–39.
2. Cristofolini, I., Menapace, C., Cazzolli, M., Rao, A., Pahl, W., & Molinari, A. (2012). The effect of anisotropic dimensional change on the precision of steel parts produced by powder metallurgy. *Journal of Materials and Processing Technologies, 7*(212), 1513–1519.
3. Menapace, C., Larsson, M., Torresani, E., Cristofolini, I., & Molinari, A. (2012). Study of anisotropy during sintering of ferrous alloys. In *Proceedings PM2012, 2012 powder metallurgy world congress and exhibition*. Yokohama.
4. Cristofolini, I., Pilla, M., Molinari, A., Menapace, C., & Larsson, M. (2012). DOE investigation of anisotropic dimensional change during sintering of iron–copper–carbon. *The International Journal of Powder Metallurgy, 48*(4), 37–43.
5. Cristofolini, I., Pilla, M., Larsson, M., & Molinari, A. (2012). A DOE analysis of dimensional change on sintering of a 3%Cr–0.5%Mo–x%C steel and its effect on dimensional and geometrical precision. *Powder Metallurgy Progress, 3*(12), 127–143.
6. Cristofolini, I., Corsentino, N., Molinari, A., & Larsson, M. (2014). Study of the influence of material and geometry on the anisotropy of dimensional change on sintering of powder metallurgy parts. *International Journal of Precision Engineering and Manufacturing, 15*(9), 1865–1873.
7. Corsentino, N., Menapace, C., Cristofolini, I., Pilla, M., Larsson, M., & Molinari, A. (2015). The influence of the liquid phase on anisotropic dimensional change on sintering of iron alloys. *The International Journal of Powder Metallurgy, 51*(2), 27–37.
8. Cristofolini, I., Pilla, M., Rao, A., Libardi, S., & Molinari, A. (2013). Dimensional and geometrical precision of powder metallurgy parts sintered and sinter hardened at high temperature. *International Journal of Precision Engineering and Manufacturing, 14*(10), 1735–1742.
9. Emanuelli, L., Menapace, C., Cristofolini, I., Molinari, A., & Larsson, M. (2014). Influence of sintering temperature on shrinkage anisotropy in Cr–Mo low alloy steel green compacts. *Advances in Powder Metallurgy and Particulate Materials, 5,* 99–107.
10. Cristofolini, I., Corsentino, N., Molinari, A., & Larsson, M. (2015). Influence of geometry and process variables on the anisotropy parameter K. *Advances in Powder Metallurgy and Particulate Materials, 01,* 31–40.
11. Corsentino, N., Cristofolini, I., Libardi, S., & Molinari, A. Effect of high sintering temperature on the dimensional and geometrical precision of PM Cr–Mo steel parts. In *Proceedings EURO PM2014 congress and exhibition, Salzburg 21–24 September 2014.* Shrewsbury: EPMA. 13_P2_EP140145.
12. Griffo, A., Ko, J., & German, R. M. (1994). Critical assessment of variables affecting the dimensional behavior in sintered iron–copper–carbon alloys. *Advances in Powder Metallurgy and Particulate Materials, 3,* 221–236.
13. Bernardo, E., Campos, M., Torralba, J. M., Gierl, C., Danninger, H., & Frykholm, R. (2013). Lean steels modified with a new Cu-based master alloy: Influence of process parameters in dimensional and sintering behavior. In *Proceedings Euro PM 2013, international powder metallurgy congress and exhibition, 15–18 September 2013.* Gothenburg.
14. De Oro Calderon, R., Gierl, C., & Danninger, H. (2016). Dimensional stability of sintered steels containing low melting point master alloys. In *Proceedings world PM 2016 congress and exhibition, 9–13 October 2016*. Hamburg.
15. Sainz, S, Bilbao, C., Veiga, A., & Castro, F. (2016). Enhanced control of dimensional change and mechanical properties of Fe–Cu–C PM steels under optimized sintering cycle. In: *Proceedings world PM 2016 congress and exhibition, 9–13 October 2016.* Hamburg
16. Bilbao, C., Sainz, S., Veiga, A., & Castro, F. (2015). Microstructural development and effect of different Cu/C contents on dimensional changes during sintering of PM steels. *Powder Metallurgy, 58*(5), 328–334.
17. Bernardo, E., Oro, R., Campos, M., Frykholm, R., Litström, O., & Torralba, J. M. (2012). Effect of liquid content on dimensional stability and sinter properties of liquid-phase sintered low alloyed steels. In *Proceedings of the international Euro powder metallurgy congress and exhibition, Euro PM 2012*, 16–19 September 2012 (Vol. 1). Basel
18. Molinari, A., Menapace, C., Torresani, E., Cristofolini, I., & Larsson, M. (2013). Working hypothesis for origin of anisotropic sintering shrinkage caused by prior uniaxial cold compaction. *Powder Metallurgy, 56*(3), 189–195.
19. Molinari, A., Torresani, E., Menapace, C., Cristofolini, I., & Larsson, M. (2013). A study of sintering shrinkage kinetics of cold compacted ferrous green parts. *Advances in Powder Metallurgy and Particulate Materials, 5,* 25–32.
20. Molinari, A., Baselli, S., Torresani, E., Cristofolini, I., & Larsson, M. (2016). The shrinkage of uniaxially cold compacted iron green parts. In *Proceedings world PM2016 congress and exhibition, Hamburg 9–13 October 2016.* Shrewsbury: EPMA. 13_P2_EP3302140.
21. Molinari, A., Bisoffi, E., Menapace, C., & Torralba, J. (2014). Shrinkage kinetics during early stage sintering of cold isostatically compacted iron powder. *Powder Metallurgy, 57*(1), 61–69.
22. Molinari, A., Torresani, E., Menapace, C., & Larsson, M. (2015). The anisotropy of dimensional change on sintering of iron. *Journal of the American Ceramic Society, 98*(11), 3431–3437.
23. Baselli, S., & Molinari, A. (2017). The geometrical model of sintering. In *CD proceedings EuroPM2017 congress and exhibition, Milano (Italy) 1–5 October 2017.* Shrewsbury: EPMA.
24. Zavaliangos, A., & Bouvard, D. (2000). Numerical simulation of anisotropy in sintering due to prior compaction. *The International Journal of Powder Metallurgy, 36*(7), 58–65.

25. Zavaliangos, A., Missiaen, J. M., & Bouvard, D. (2006). Anisotropy in shrinkage during sintering. *Science of Sintering, 38,* 13–25.
26. Torresani, E., Cristofolini, I., & Molinari, A. (2015). Study of the anisotropic microstructure of the uniaxially cold compacted green parts. *Advances in Powder Metallurgy and Particulate Materials, 3,* 9–18.
27. Molinari, A., Amirabdollahian, S., Cristofolini, I., & Federici, M. (2016). Influence of powder deformation on anisotropy of sintering shrinkage. *Advances in Powder Metallurgy and Particulate Materials, 1,* 45–52.
28. Molinari, A., Zago, M., Amirabdollahian, S., Cristofolini, I., & Larsson, M. (2017) Anisotropic sintering shrinkage of ring shaped iron parts: effect of geometry and green density and correlation to the stress field during uniaxial cold compaction. In *Proceedings EURO PM2017 congress and exhibition, Milan 1–4 October 2017.* Shrewsbury: EPMA. 33686349.
29. Amirabdollahian, S., Deirmina, F., & Molinari, A., Study of the pores characteristics in the uniaxially cold compacted green parts by image analysis. In *CD proceedings world PM2016 Hamburg (Germany) 9–13 October 2016*. Shrewsbury: EPMA.
30. Molinari, A., & Torresani, E. (2015). Preliminary study to determine the sintering stress from microstructural analysis of green parts. *Powder Metallurgy, 58*(5), 323–327.
31. Olevsky, E. A. (1998). Theory of sintering: From Discrete to Continuum. *Materials Science and Engineering Reports, 23,* 41–100.
32. Bordia, R. K., Zuo, R., Guillon, O., Salamone, S. M., & Rodel, J. (2006). Anisotropic constitutive laws for sintering bodies. *Acta Materialia, 54,* 111–118.
33. Wakai, F., Chihara, K., & Yoshida, M. (2007). Anisotropic shrinkage induced by particle rearrangement in sintering. *Acta Materialia, 55,* 4553–4566.
34. Wakai, F., & Shinoda, Y. (2009). Anisotropic sintering stress for sintering of particles arranged in orthotropic symmetry. *Acta Materialia, 57,* 3955–3964.
35. Cristofolini, I., Corsentino, N., Pilla, M., Molinari, A., & Larsson, M. (2013). Influence of geometry on the anisotropic dimensional change on sintering of PM parts. *Advances in Powder Metallurgy and Particulate Materials, 11,* 49–61.
36. Raman, R., Zahrah, T. F., Weaver, T. J., & German, R. M. (1999). Predicting dimensional change during sintering of FC0208 parts. *Advances in Powder Metallurgy and Particulate Materials, 1*(3), 115–122.
37. Corsentino, N., Cristofolini, I., Larsson, M., Libardi, S., & Molinari, A. (2015). Anisotropy of the dimensional variation of sintered parts: a predictive model and a statistical evaluation of its reliability. In *Proceedings EURO PM2015 congress and exhibition, Reims 4–7 October 2015*. Shrewsbury: EPMA. 3213322.
38. Cristofolini, I., Corsentino, N., Molinari, A., & Larsson, M. (2014). A design procedure accounting for the anisotropic dimensional change on sintering of ferrous PM parts. *Advances in Powder Metallurgy and Particulate Materials, 01,* 115–127.
39. ISO 10360-4. (2000). Geometrical product specifications (GPS)—Acceptance and reverification tests for coordinate measuring machines (CMM)—Part 4: CMMs used in scanning measuring mode.

I. Cristofolini is Associate Professor in the field of Design Methods for Industrial Engineering at the University of Trento - Department of Industrial Engineering (Italy). Main research areas: Design for Powder Metallurgy, Design against wear, Geometric Dimensioning and Tolerancing, Knowledge-Based Design systems.

A. Molinari is Full Professor of Metallurgy, University of Trento (I). Honorary PhD - Universidad Carlos III, Madrid; Fellow of EPMA - European Powder Metallurgy Association; Fellow of APMI - American Powder Metallurgy Institute. Main research areas: Powder Metallurgy, Additive Manufacturing, Wear of metallic materials.

M. Zago is PhD student in Material, Mechatronics and Systems Engineering at the University of Trento (I). He received the MSc in Materials Engineering in 2016 and BSc in Industrial Engineering in 2013 from the University of Trento. Main research areas: compaction mechanics, design for sintering.

S. Amirabdollahian is a doctoral researcher at the University of Trento, Italy. He received the MSc in Materials Engineering in 2014 from the University of Trento. Main research areas: powder metallurgy, additive manufacturing of metals using laser metal deposition.

O. Coube has been coordinating for more than 24 years Projects between Universities, R&D Centres, Industries and Associations. PhD and Project Manager in a Fraunhofer Institute in Germany. Since 2007 Technical Director in a UK based European Trade Association of a Metallurgical Sector.

M. J. Dougan is Chief Metallurgist in the AMES PM Tech Centre, working on material and process development, failure analysis, and soft magnetic materials. He received his BSc and PhD in Metallurgy from the University of Manchester in 1991 and 1995 respectively.

M. Larsson is Senior Development Engineer at Global Technology department at Höganäs AB, where he has worked within the development department since 1988. His BS degree in mechanical engineering is from Lund University. He is also chairman of ISO TC119 "Powder Metallurgy" standardization committee.

M. Schneider is Manager Modelling, Simulation & Fatigue at GKN Sinter Metals Engineering GmbH. He has a degree in mechanical engineering and quality engineering from the University of Wuppertal. He received his PhD in fracture mechanics from the University of Wuppertal.

P. Valler is Innovation Project Leader at Sintex, developing new shaping techniques and alloys for powder metal as well as magnets, soft magnetic materials and magnetic systems. He has a degree in Export Engineering specialized in Global Business Development from Aalborg University.

J. Voglhuber is Development Engineer in the R&D Material Team at Miba Sinter Austria GmbH, where he has worked since 1997. He has a degree in Automation Engineering from Higher technical college in Wels/Austria.

L. Wimbert is Director Materials Development Powder Metallurgy at Hoeganaes Corporation Europe. He received his PhD in Inorganic Chemistry from Technical University of Dortmund. Up to 2018 he was Director Process Technology at GKN Sinter Metals Engineering.